Plant Soil (2014) 377:277–293
DOI 10.1007/s11104-013-1990-8

REGULAR ARTICLE

Linking transpiration reduction to rhizosphere salinity using a 3D coupled soil-plant model

Natalie Schröder · Naftali Lazarovitch · Jan Vanderborght · Harry Vereecken · Mathieu Javaux

Received: 19 September 2013 / Accepted: 21 November 2013 / Published online: 28 December 2013

Abstract
Aims Soil salinity can cause salt plant stress by reducing plant transpiration and yield due to very low osmotic potentials in the soil. For predicting this reduction, we present a simulation study to (i) identify a suitable functional form of the transpiration reduction function and (ii) to explain the different shapes of empirically observed reduction functions.
Methods We used high resolution simulations with a model that couples 3D water flow and salt transport in the soil towards individual roots with flow in the root system.
Results The simulations demonstrated that the local total water potential at the soil-root interface, i.e. the sum of the matric and osmotic potentials, is for a given root system, uniquely and piecewise linearly related to the transpiration rate. Using bulk total water potentials, i.e. spatially and temporally averaged potentials in the soil around roots, sigmoid relations were obtained. Unlike for the local potentials, the sigmoid relations were non-unique functions of the total bulk potential but depended on the contribution of the bulk osmotic potential.
Conclusions To a large extent, Transpiration reduction is controlled by water potentials at the soil-root interface. Since spatial gradients in water potentials around roots are different for osmotic and matric potentials, depending on the root density and on soil hydraulic properties, transpiration reduction functions in terms of bulk water potentials cannot be transferred to other conditions, i.e. soil type, salt content, root density, beyond the conditions for which they were derived. Such a transfer could be achieved by downscaling to the soil-root interface using simulations with a high resolution process model.

Keywords Soil-root modelling · Salinity · Root water uptake · Stress function

Responsible Editor: Rafael S. Oliveira.

N. Schröder (✉) · M. Javaux
Forschungszentrum Jülich GmbH, Institute of Bio- and Geoscience Agrosphere Institute, IBG-3, 52425 Jülich, Germany
e-mail: na.schroeder@fz-juelich.de

N. Schröder
Department of Hydromechanics and Modelling of Hydrosystems, Institute for Modelling Hydraulic and Environmental Systems, University of Stuttgart, Pfaffenwaldring 61, 70569 Stuttgart, Germany

M. Javaux
Earth and Life Institute/Environmental Sciences, Universite catholique de Louvain, Croix du Sud, 2, L7.05.02, 1348 Louvain-la-Neuve, Belgium

N. Lazarovitch
Wyler Department for Dryland Agriculture, French Associates Institute for Agriculture and Biotechnology of Drylands, Jacob Blaustein Institutes for Desert Research, Ben-Gurion University of the Negev, Sede Boqer Campus, 84990 Midreshet Ben-Gurion, Israel

J. Vanderborght · H. Vereecken
Forschungszentrum Jülich GmbH, Institute of Bio- and Geoscience, Agrosphere Institute (IBG-3)/Centre for High-Performance Scientific Computing in Terrestrial Systems TerrSys, Jülich 52425, Germany

Introduction

Irrigation of agricultural lands uses 70 % of the global fresh water withdrawals (Siebert et al. 2010) and is necessary, especially in arid and semi-arid areas, to increase and optimize crop production. The high demand and water quality decline in many regions require a careful and economical handling of the available water resources. One major problem of irrigated fields is the soil salinity (Bhantana and Lazarovitch, 2010). Salts accumulate in the root zone and at the soil surface and cause high osmotic potentials in the soil, which lead to very low values of the water potential near the plant roots (Hamza and Aylmore 1992). Plants suffering from salt stress respond by reducing their transpiration rate, and thus their yield (de Wit 1958).

Soil-hydrological models may be used to predict plant responses to salt stress. In these models, a potential transpiration rate T_{pot}, which corresponds to transpiration under optimal growing conditions, is defined and distributed as a water sink term over the root zone, commonly as a function of the root length density. If the potential atmospheric demand cannot be supplied by the plant, due to too much/little water and/or too much salt in the soil, the transpiration is reduced. In a soil hydrological context, this reduction is defined as a plant stress.

In a first type of models, called type II models (Hopmans and Bristow 2002), the stress response function α is defined as a function of matric water potential and/or the osmotic potential in the root zone. The stress response function links a whole plant response (described by relative yield and/or relative transpiration) to salts and water in the root zone, as

$$\frac{Y_{act}}{Y_{pot}} \; or \; \frac{T_{act}}{T_{pot}} = \alpha \tag{1}$$

where Y_{act} is an actual yield, Y_{pot} is a potential yield, T_{act} is an actual transpiration rate, and T_{pot} is a potential transpiration rate. Several stress response functions have been developed over the years (Homaee et al. 2002a; Feddes and Raats 2004), whereas two mathematical formulations are most common for stress functions: piecewise linear for salt stress (Maas and Hoffman 1977) and for water stress (Feddes et al. 1976) and *s*-shaped functions for water and salt stress (van Genuchten and Hoffman 1984; van Genuchten 1987), but other modified functions exists (Feddes and Raats 2004). Salt and water stress response functions were often developed independently. If a combination of both stress types is described, salt and water response functions are added (osmotic and matric potential), multiplied (stress response for salt and water) or otherwise recombined (Homaee et al. 2002b). The right way to combine two stress functions has been subject of discussion in the literature (Homaee et al. 2002c; Hopmans and Bristow 2002; Feddes and Raats 2004).

However the use of such stress functions and their combination has been criticized. Water and salinity stress functions must link the response of the whole plant, i.e. transpiration rate or yield, to matric and osmotic water potentials in the root zone, which vary considerably with depth, with horizontal distance to roots and with time. A typical approach is to infer the whole plant response from a composite of local stress responses, which are derived from local soil matric and osmotic potentials. However, since the root system is hydraulically connected the local response of the system does not depend solely on the local conditions but also on the conditions at other locations in the root zone (Skaggs et al. 2006). In case of heterogeneous soil matric potential, for instance, a local reduction of water uptake may be compensated by an increase in water uptake at other depths where sufficient water is still available (Jarvis 2011). Applying local stress functions without a link to conditions at other locations in the root zone may therefore lead to errors in simulated water uptake distributions.

Another potential weakness of type II models arises from the fact that bulk soil (and not soil-root interface) water potentials are used in stress functions. Water uptake by a single root creates a radial water potential gradient towards and salt accumulation at the soil-root interface so that the water potential at the interface differs from bulk soil water potential. The difference depends on the soil hydraulic properties, the uptake rate, and the root density. We postulate that the gradients of matric potential and the gradients of osmotic potential between bulk soil and soil-root interface will be different as well. Since water potentials at the soil-root interface are relevant for plant stress, stress functions defined in terms of bulk soil water potentials should be functions of soil hydraulic properties, root densities, water uptake, and also of the type of stress (i.e. matric versus osmotic stress). These dependencies should be parameterized in stress functions of type II models.

In addition to type II models, Hopmans and Bristow (2002) also defined type I models in which the water

flow in the soil-root system is described in a mechanistic manner and based on water potential differences/gradients and conductances/conductivities along a flow line in the soil-plant system. The major advantages of this modeling approach are that local processes between the bulk soil and the soil-root interface and hydraulic connections in three-dimensional root architecture are simulated explicitly based on principal laws of water flow in porous media (the root tissue can also be considered as a porous medium). Type I models therefore avoid empirical parameterizations of root water uptake, uptake compensation, and stress functions that are used in type II models. Simulations using type I models can be used to derive parameterizations for type II models. Metselaar and de Jong van Lier (2007), de Jong van Lier et al. (2008), and Couvreur et al. (2012) used type I models to parameterize root water uptake functions for the case of matric potential stress.

For combined matric and osmotic potential stresses, Cardon and Letey (1992) compared the sensitivity of type I and type II models. They used the type I water uptake model of Nimah and Hanks (1973) and concluded that it was insensitive to osmotic stress, while the type II model (zero-to-one stress function) produced, when compared with experimental data, more reasonable results. The Nimah and Hanks (1973) model calculates the radial water flow into the root based on the difference between the bulk soil water potential and the water potential in the root. Yet, the accumulation of salts at the soil-root interface was not considered in the model, which may be a reason for the small sensitivity of the used type I model to bulk soil osmotic potentials. Therefore, we refined the model and considered also three-dimensional (3D) water and salt transport in the soil towards the 3D root architecture so that water flow into the root can be modeled based on the potential difference between the potential at the soil-root interface and inside the root.

The objectives of the study are (1) to investigate how the stress functions used in type II models depend on the total water potential and its partial potentials: matric and osmotic potentials, and on the transpiration rate, and (2) to analyze stress responses as a function of water potentials at the soil-root surface and in the bulk soil. Therefore, we carried out simulations using the type I model R-SWMS (Javaux et al. 2008), which considers 3D flow and transport in the coupled soil-root system.

We hypothesize that the local water potential at the soil-root interface, which is 'felt' by the plant, is the key to a unique stress function for salt and water stresses, assuming there is no plant osmotic adjustment. We further assume that a perfect osmotic membrane is present in the roots, which separates water in the root conductive tissue (xylem) from soil water. We hypothesize that this assumption implies that how the local water potential at soil-root interface is made up by osmotic and matric potentials is irrelevant for root water uptake. However, the different spatial distributions of the matric potential and the osmotic potential around individual roots lead to different sensitivities of water uptake to bulk matric or osmotic potentials, when potential gradients occur. Therefore, we hypothesize that at the macroscopic scale, the effect of the bulk osmotic potential on root water uptake will be different from the effect of the bulk matric potential.

First, we compare experimental data from measurements by Hamza and Aylmore (1992) with simulated data to validate our model and assumption of a perfect osmotic membrane. In their experimental setup, salt accumulation of Na^+ at the root surface of a lupine plant was detected with Na^+-LIX microelectrodes. In addition, leaf water potential and the actual transpiration rate were measured. Different simulation runs were performed based on these experimental setups with four saline treatments and the experimental and simulated data are compared. In a second step, a simple simulation setup, consisting of one vertical root in the middle of a soil cube, was considered. In this setup, scenarios with different salinities and potential transpiration rates were defined in order to analyze the transpiration response to local soil water potential. Finally, a more realistic case was simulated for a root system typical of grassland to assess the impact of more complex root architectures on a one-dimensional (1D) effective salt stress function.

Theory

The total water potential is equal to

$$H = h + z + h_o, \tag{2}$$

where H is the total water potential, h is the matric potential, z is the gravitational potential, and h_o is the osmotic potential. In soil hydrology, potentials are mostly defined on a weight basis (heads) and these have dimension of length. In plant sciences, potentials are mostly defined on a volume basis and have dimension

of a pressure. Heads can be simply translated to pressures by multiplying the head by $\rho_w g$ where ρ_w is the density of water and g the acceleration due to gravity. We use for potentials dimension [cm] in the following, which approximately corresponds with pressure in [hPa = 10^2 Pa].

It should be noted that osmotic potential gradients only drive liquid water flow when salt movement is restricted compared with the movement of water molecules. This might be the case for flow across selective membranes such as plant cell membranes or through thin water films in porous media in which the mobility of hydrated ions is restricted (Nassar and Horton 1997). For the cases considered here, we will neglect water flow due to gradients in osmotic potential in the soil.

Based on this definition of the total water potential and on analytical solutions of water flow in a root system, Couvreur et al. (2012) developed a new model of plant water stress. In their model, water stress and compensatory root water uptake are clearly decoupled and an explicit equation for the actual transpiration rate T_{act} [cm^3 d^{-1}] is proposed as:

$$T_{act} = K_{rs}\left(\sum_{j=1}^{M} H_{si,j}SSF_j - H_{collar}\right) \quad (3)$$

where K_{rs} [cm^3 cm^{-1} d^{-1}] is the equivalent conductance of the complete root system, M [−] is the total number of soil elements, $H_{si,j}$ [cm] the total water potential at the soil-root interface in a soil compartment j, H_{collar} [cm] the water potential at the root collar, and SSF_j [−] is the standard sink fraction in the j-th soil element. The vector of standard sink fractions, SSF, represents the distribution of the normalized sink terms in the soil domain for the case of a uniform soil water potential distribution in the soil profile. The SSF_j depends on the root system architecture and its hydraulic properties and is obtained by solving the flow equation in network of root segments for a uniform water potential at the soil-root interface (Doussan et al. 1998; Couvreur et al. 2012). The term $\sum_{j=1}^{M} H_{si,j}SSF_j$ is the SSF-weighted mean soil water potential at the soil-root interface and represents the plant-sensed soil water potential. If no salinity is considered, the water potential is the sum of matric and elevation potential ($H=h+z$), while with salinity, the osmotic potential is added ($H=h+z+h_o$).

Stress in this model is defined to occur when H_{collar} reaches a predefined value, $H_{collar,crit}$ below which H_{collar} cannot fall due to leaf stomatal regulation. In this case, T_{act} can be calculated from Eq. (3) for the soil water potential distribution and the water potential at the root collar.

Dividing Eq. (3) by T_{pot} [cm^3 d^{-1}], the transpiration reduction factor can be estimated as

$$\alpha = \frac{T_{act}}{T_{pot}} = \frac{K_{rs}}{T_{pot}}\left(\sum_{j=1}^{M} H_{si,j}SSF_j - H_{collar,crit}\right). \quad (4)$$

For $H_{collar} > H_{collar,crit}$ the potential atmospheric demand can be fulfilled and α is equal to 1 ($T_{act}=T_{pot}$). In case of $H_{collar} = H_{collar,crit}$, water uptake by the plant is reduced linearly to the plant 'felt' soil water potential. Since they link the whole plant response, i.e. transpiration rate to an averaged soil water potential, Eqs. (3) and (4) give some indications about the shape of type II models. According to Eqs. (3) and (4), the transpiration reduction should be a function of the sum of local matric and osmotic potentials and should be independent of the nature of the partial water potential that generates stress. This contradicts type II models that use products of stress response functions to, respectively, matric and osmotic potentials, e.g. HYDRUS-1D (Simunek et al. 2013), SWAP (Kroes et al. 2008) or HYSWASOR (Dirksen et al. 1993). Equations (3) and (4) also indicate that the reduction functions should be linear functions with a slope that depends on root properties, K_{rs}, the potential transpiration rate, T_{pot}, but is independent of soil properties. However, the water potential in Eqs. (3) and (4) is defined at the soil-root interface and is therefore a local variable that may differ from the bulk averaged water potential at a certain depth in the soil profile. In the following, we will use detailed 3D simulations of water flow and salt transport in the soil towards roots and inside the root system in a saline soil. The simulation results are used subsequently to evaluate the shape of reduction functions when water potentials are determined as an average of the potentials in the bulk soil around roots.

Methods and materials

Modeling

We used the simulation model R-SWMS (Javaux et al. 2008) that solves the 3D Richards equation (Richards 1931) to describe water flow in the soil and the Doussan equations (Doussan et al. 1998) to describe water flow

inside and into the plant roots. These equations describe fluxes in the root network based on pressure potential differences across a membrane between the soil-root interface and the root xylem, pressure potential gradients along root segments, and radial and axial root conductance or conductivities. Solute transport in the soil is modeled by the 3D convection–dispersion equation (CDE) and solved with a particle tracking algorithm (Bechtold et al. 2011; Schröder et al. 2012). Since the transport influences osmotic potentials and therefore root water uptake, the transport process has an impact on the flow. This back-coupling between water flow and solute transport within one time step was implemented in an explicit way, using the solute concentrations (transformed to osmotic potentials) at the beginning of one time-step to calculate the radial flows at the soil-root interface. More details of the coupling of the different model modules are given in the Appendix.

The water potential difference between the soil and the root xylem in a certain root segment j is considered to be the sum of two components: h and h_0. The radial flow into the root segment j is described using the following equation (Hopmans and Bristow 2002)

$$J_r^j = K_r^* A_r\left(\left(h_{int} - h_{xylem}\right) + \sigma\left(h_{o,int} - h_{o,xylem}\right)\right), \qquad (5)$$

where K_r^* [cm d^{-1} cm^{-1}] is the radial root conductance, A_r [cm^2] is the root outer surface, h_{int} [cm] and $h_{o,int}$ [cm] are the pressure and the osmotic potentials at the soil–root interface, and h_{xylem} [cm] and $h_{o,xylem}$ [cm] are the pressure and the osmotic potentials in the xylem.

The reflection coefficient σ can vary between zero and one and represents the effectiveness of the membrane complex to selectively allow water flow but no salt transport across the complex so that osmotic potential gradients may drive a water flow across the membrane (Hopmans and Bristow 2002). Note that we consider in all simulations that the root endodermis acts as a perfect membrane with a reflection coefficient $\sigma = 1$ (Knipfer and Fricke 2010). As mentioned before, the potentials at the interface h_{int} and $h_{int,o}$ are defined locally as the matric and osmotic potential in the soil voxel around a given root segment. In our definition, we neglect the osmotic potential inside the xylem $h_{o,xylem}$ and assume it is zero, which means that we also neglect any plant osmotic adjustment. However, a plant osmotic potential could be implemented in the model straightforwardly. Considering an osmotic potential in the xylem will lead to an uptake that is similar to an uptake from a less saline soil solution. Therefore, it will not influence fundamentally the conclusions drawn from simulation results that are obtained without considering the xylem osmotic potential.

Plant stress was defined in the model by setting a critical stress value of $H_{collar,crit} = -15{,}000$ cm (≈ -1.5 MPa) at the root collar, to simulate an isohydric plant behavior (Tardieu 1996). When the collar potential reaches $H_{collar,crit}$, the boundary condition (BC) at the root collar switches from a flow BC (transpiration rate) to a constant potential BC equal to $H_{collar,crit}$. After this switch, the actual transpiration rate T_{act} is reduced compared to the potential (applied) transpiration rate T_{pot}. When the potential transpiration demand can be fulfilled again by the total root water uptake (e.g., due to more available water in the soil or a decrease of T_{pot}), the BC type is switched back applying the potential transpiration flux at the root collar.

Simulation setup

Three scenarios were run in this study. The first one aimed at validating our model by comparing simulation results to data from the literature. A second setup allowed us to investigate the sensitivity of the effective reduction function obtained from the 3D model to osmotic and matric potentials at the soil-root surface and in the bulk soil, and to the transpiration rate. Finally, a larger scale scenario was run with a more realistic plant root structure to investigate the impact of root distribution on effective stress functions. The simulation results are evaluated based on the approach of Couvreur et al. (Eqs. (3) and (4)).

Calculation of matric and osmotic potentials

The salt concentration c [μmol cm^{-3}] in the model was transferred to the osmotic potential h_o [cm] according to

$$h_O = \beta c$$

with $\beta = -50\frac{cm^4}{\mu mol}$. The parameter β was calculated from data of Shani and Ben-Gal (2005) and Hamza and Aylmore (1992).

The water potential at the soil-root interface was computed for the complete root domain as a weighted average of potentials in all soil voxels that contain one or more root segments. The voxel size was assumed to be small enough (see further for details about the voxel

size) so that the water potential in the voxel represents the water potential at the soil-root interface. Bulk soil water potential for the whole soil domain was calculated as a weighted average of potentials in all voxels of the soil domain. For both, the soil-root interface and bulk soil average water potentials, the standardized sink fractions (*SSF*) were used as weights. Since the *SSF* is only defined in soil voxels containing a root segment, water potentials in voxels further away from roots were weighted by the *SSF* of the nearest voxel containing a root segment.

In addition, the average value of all voxels at a certain distance to the nearest root was calculated. Doing this for different distances, the spatial variation of water potential in the radial direction to the root segments was derived.

Scenario 1: comparison to hamza and aylmore dataset

In the first simulation setup, a soil column of 4.5×4.5×12 cm with 0.5 cm grid spacing, was defined so as to compare the simulation results with measured data from Hamza and Aylmore (1992). In their experiment, salt accumulation of Na^+ at the root surface, leaf water pressure potential and the actual transpiration rate of a lupine plant with a single root were measured. The water retention curve and diffusivity function of the used soil (85 % Bassendean sand and 15 % Clackline kaolinite form Western Australia) were measured by Hainsworth and Aylmore (1986). The parameters of the Mualem-van Genuchten (MvG) hydraulic functions (van Genuchten 1980) were obtained by fitting using the RETC software (van Genuchten et al. 1991) and are given in Table 1 (R^2=0.907).

A single plant root with a total length of 12 cm was located in the center of the box. The hydraulic characteristics of the roots were assumed to be constant over time and uniform along the root. The root axial conductance was set to $K_x = K_x^* A_x = 0.2592$ cm^4 d^{-1} cm^{-1} and a radial conductivity K_r^*, equal to 0.000864 cm d^{-1} cm^{-1} was assumed, based on measured values of lupine roots by Doussan et al. (2006). Plant transpiration rates measured by Hamza and Aylmore (1992) were used as collar boundary condition and four treatments with different initial salt concentration in the soil (c_{init}=25, 50, 75, 100 μmol cm^{-3}) were simulated. Analogous to their experimental setup, no infiltration and no outflow were defined and the initial water content was θ_{init}= 0.3 cm^3 cm^{-3}. Simulation outputs were compared to the experimental data at 2, 4, 6, and 8 h after the start of the experiment similarly to their study. We assumed that the water potential at the root collar is a good proxy of the leaf water potential (pressure potential loss in the stem was considered as negligible).

With this comparison, we verified whether our assumptions of no osmotic adjustments and a constant reflection coefficient of σ=1 are valid. Therefore, we started from the following general function to describe the relation between T_{act}, leaf pressure potential h_{leaf}, osmotic potential and matric potential (see Eq. 3):

$$T_{act} = K_{eff}\left[|h|_{leaf} - \sigma\left(|h|_{o,int} - |h|_{o,xylem}\right) - |h|_{int}\right] \quad (6)$$

This can be rewritten as

$$T_{act} = K_{eff}\left[|h_{leaf}| - |h_{int}| - |h_{o,int}|\right] + K_{eff}(1-\sigma)|h_{o,int}| + K_{eff}\sigma|h_{o,xylem}| \quad (7)$$

When we assume that σ = 1 and that $h_{o,xylem}$ is 0, then T_{act} versus $|h_{leaf} - h_{o,int} - h_{int}|$ for all salt concentrations should fall on the same line through the origin and the slope should be equal to K_{eff}. If σ=1 but $h_{o,xylem}$ is different from 0, T_{act} plotted versus $|h_{leaf}| - |h_{o,int}| - |h_{int}|$ results in a line but with a non-zero intercept. If the osmotic potential has less influence on root water uptake (σ<1), or does not play any role (σ=0), then T_{act} versus $|h_{leaf}| - |h_{int}|$ should be a line through the origin for all salt concentrations.

Scenario 2: simulated stress function with a single root

In this scenario we analyzed the plant stress response due to salt accumulation around roots using a very simplified simulation setup with a single root only, which is similar to the experimental setup of Hamza and Aylmore (1992). The defined setup geometry for the single root setup is shown in Fig. 1a. The soil column geometry was 4.5×4.5×10 cm, discretized with 0.5 cm cubes. The soil column was filled homogeneously with clay loam (MvG-parameters in Table 1).

The single plant root had a total length of 8 cm and was placed in the center of the box, leading to a root length density (RLD) of 0.04 cm cm^3. Axial root conductance were set to $K_x = K_x^* A_x = 0.0432$ cm^4 d^{-1} cm^{-1} and the radial conductivity was set to K_r^*=0.000178 cm d^{-1} cm^{-1} (Doussan et al. 1998). The root hydraulic characteristics were assumed to be constant over time and uniform along the root. As root boundary condition, three different constant potential transpiration rates

Table 1 Mualem-van Genuchten parameter for the different simulation scenarios

	θ_r $cm^3\ cm^{-3}$	θ_s $cm^3\ cm^{-3}$	α cm^{-1}	n –	l –	K_s $cm\ d^{-1}$	Scenario
(Hainsworth and Aylmore 1986)	0.001	0.432	0.00285	2.867	0.355	0.723	1
Clay loam	0.095	0.41	0.019	1.31	0.5	6.24	2,3

(T_{pot}=1.0, 1.5, 2.0 $cm^3\ d^{-1}$) were applied at the root collar. Considering a 1 m long root in a vertical soil column with a surface area of 4.5×4.5 cm^2, an uptake rate of 1 $cm^3\ d^{-1}$ from a 8 cm long root segment would correspond with 12.5 cm^3 for the total root, or a transpiration rate of 6 mm d^{-1}.

At all boundaries (top, bottom, left, right, front, back) a no flux condition for water flow simulation and a reflection condition for the particle tracking was set during the simulations. The initial pressure potential was h_{init}=−1,000 cm and the initial solute concentration c_{init} in the soil solution varied between different scenarios (5, 10, 20, 30, 60, 90, 120, 150, 200, 250 µmol cm^{-3}), and were always defined uniform over the soil domain. The longitudinal dispersivity length α_L was set to 1 cm and the transverse dispersivity length to α_T=1/10 α_L. The diffusion coefficient D_W of salt in free water was 1 $cm^2\ d^{-1}$. The simulation period was 6 days.

Scenario 3: stress functions for a full root architecture

As we expected that root spatial distribution could impact the apparent stress function, a setup with whole plant architecture was simulated. Therefore, a 25-day-old plant root architecture was set centered in a soil domain (Fig. 1b). This architecture was created with RootTyp (Pagès et al. 2004), based on parameters for Italian ryegrass (*Lolium multiflorum* L., in Schröder et al. 2012). The soil domain was 6.5×6.5×10 cm, which resulted in the root length density profile shown in Fig. 1c.

For this root system, axial root conductance, radial root conductivity, and the limiting pressure potential at the root collar were identical to the single root simulations and constant in time and branching order. In x- and y-directions of the soil domains, periodic boundary conditions were defined for soil water and solute transport, as well as for the root architecture and the root water flow (Schröder et al. 2012). In this system, the root branches that leave the soil boundary on one lateral boundary enter the domain again from the opposite boundary. This system is closer to field conditions, as boundary effects of a closed soil pot are prevented and the re-entered root branches are interpreted as branches from neighboring plants.

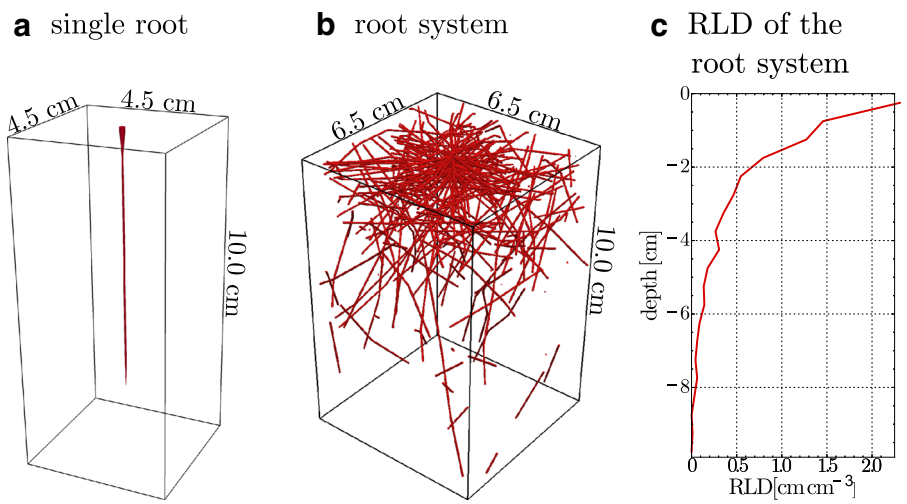

Fig. 1 Root architectures and soil geometry of **a** the single root setup and **b** the plant root structure (25 days old); **c** Root length density (RLD) of the plant root architecture (25 days old)

We assumed an irrigation with saline water before the simulation begun, and started with wet but saline soil defining a uniform initial matric potential h_{init}=−300 cm and a uniform initial soil solution concentration of c_{init}= 30 μmol cm^{-3}. The daily potential transpiration rate was T_{pot}=20 cm^3 d^{-1} and applied as sinusoidal day-night circle. The simulation period was set to 10 days.

Results and discussion

Scenario 1: comparison to hamza and aylmore dataset

The measured (Hamza and Aylmore 1992) and simulated response of leaf water potential h_{leaf} to osmotic potential h_o at the root surface (Fig. 2a), the concentration accumulation at the root surface over time (Fig. 2b), and the relation of transpiration rate T_{pot} (water uptake rate) to leaf water potential h_{leaf} (Fig. 2c) are shown for different initial soil water salinities.

The simulated concentration and osmotic potential values are in a good agreement with the experimental data, especially considering the fact that the input parameters and properties for soil and roots were imposed without any further adjustment. Slight differences may occur due to the sampling at different layers, which leads to concentration and osmotic potential values at a single point at the root surface. In contrast, the simulated values are averaged values along the whole root profile.

Absolute values of simulated h_{leaf} slightly underestimated the measured data (not negative enough) for the treatments with higher concentrations (75 and 100 μmol cm^{-3}), but showed the same trend with osmotic potential, time, and actual transpiration rate as the measured data. In the model, the potential at the root collar was assumed to represent h_{leaf} (Fig. 2c). The underestimation of the absolute leaf water potential might be due to the fact that we do not consider the potential loss in the stem or in the leaf. In addition, the relation of h_{leaf} and transpiration rate depends on the hydraulic conductivity of the plant root. Here, hydraulic properties were not measured and we assumed values from literature, which might not match exactly.

However, the comparison between measured and simulated data shows that the changes in h_{leaf} depend on the initial osmotic potential and that the changes of the salt concentration at the soil-root interface and the osmotic potential over time are well reproduced by the model simulations. In addition, the results imply that our assumptions of no osmotic adjustments and a constant reflection coefficient of σ=1 did not invalidate the model. In Fig. 3, the difference between h_{leaf} and h_{int}+h_o ($\Delta h = h_{leaf} - h_{int} - h_o$) and the difference between h_{leaf} and h_{int} ($\Delta h_{leaf,m} = h_{leaf} - h$) are plotted against T_{act} for scenarios with a reflection coefficient of σ=1.0

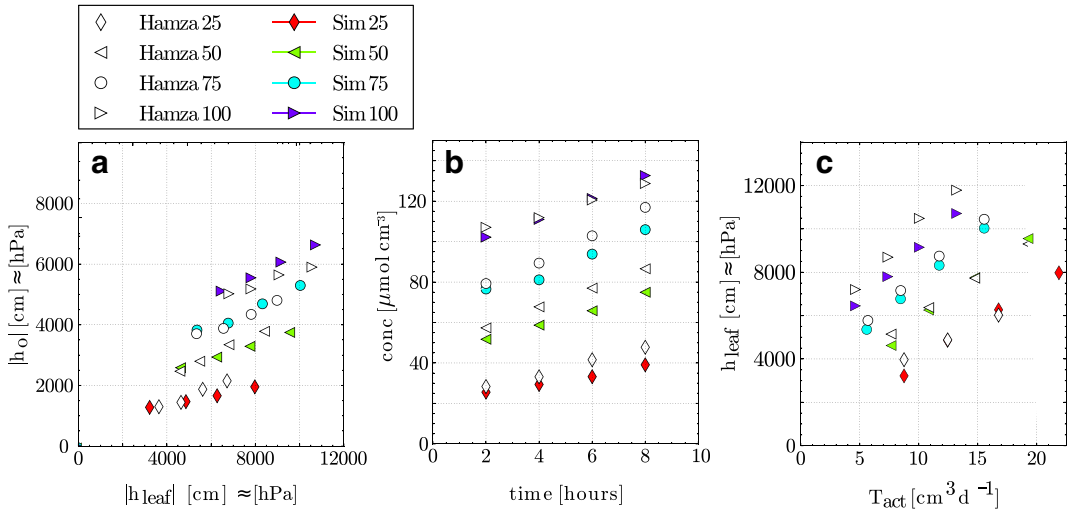

Fig. 2 Comparison of simulated data (*colored filled symbols*) and measured data (*open symbols*) from (Hamza and Aylmore 1992) for different initial salt concentrations (25, 50, 75 and 100 μmol cm^{-3}): **a** leaf water potential h_{leaf} against osmotic potential h_o at the root surface; **b** concentration accumulation at the root surface over time; **c** actual transpiration rate T_{pot} against h_{leaf}

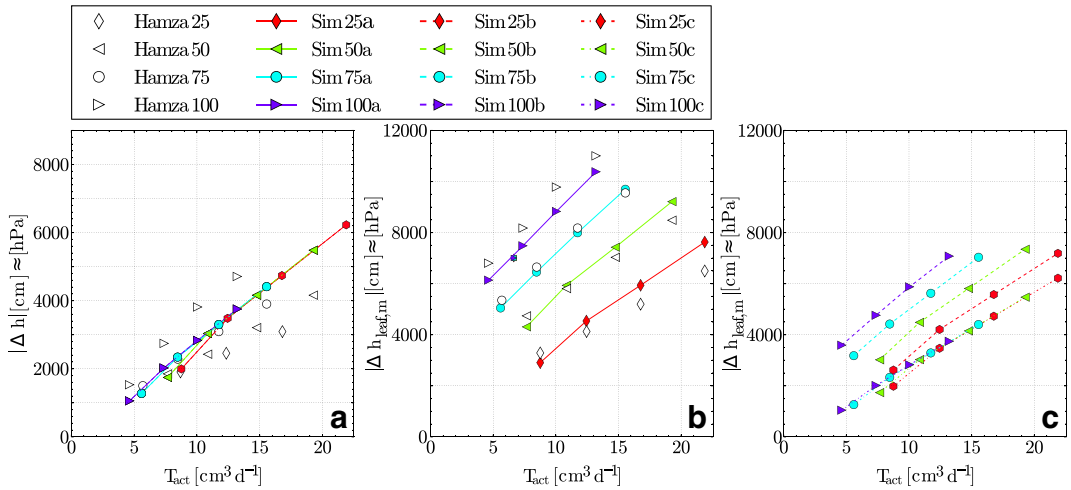

Fig. 3 **a** Δh ($h_{leaf} - h_o - h_{int}$) plotted against T_{act} for σ=1.0 and different initial salt concentrations (25, 50, 75 and 100 μmol cm^{-3}), *open symbols* are measured data from Hamza and Aylmore 1992 and *colored filled symbols* connected by *lines* are simulation results; **b** simulated *filled symbols* connected by *full lines*) and measured (*open symbols*) $\Delta h_{leaf,m}$ ($h_{leaf} - h_{int}$) plotted against T_{act} for σ=1.0; **c** simulated $\Delta h_{leaf,m}$ ($h_{leaf} - h_{int}$) plotted against T_{act} for σ=0.5 (*dashed line*) and σ=0.0 (*dotted line*)

(legend—a), σ=0.5 (legend—b) and σ=0.0 (legend—c) (see also Eq. (6)).

Figure 3 shows that the simulated difference of Δh versus T_{act} leads to a straight line through the origin with a slope of K_{eff} for all salt concentration. The data of Hamza and Aylmore (1992) show also straight lines through the origin, but the slope varies between the treatments. This indicated that K_{eff} of the root differed between the treatments. Figure 3b shows $\Delta h_{leaf,m}$ plotted against T_{act} for σ=1.0 together with the experimental data. In Fig. 3c, simulated $\Delta h_{leaf,m}$ and T_{act} are plotted against each other for σ=0.5 (dashed lines) and for σ=0.0 (dotted lines). The deviations between measured and simulated $\Delta h_{leaf,m}$ versus T_{act} relations for σ=1 (Fig. 3b) are small when compared with the differences between simulated $\Delta h_{leaf,m} - T_{act}$ relations for other σ values (σ=0.5 and σ=0 in Fig. 3c) For σ significantly smaller than 1.0, $\Delta h_{leaf,m}$ decreases due to smaller effects of the osmotic potential (Fig. 3c, dashed line, σ=0.5). Using a reflection coefficient of σ=0.0 (Fig. 3c, dotted line), the $\Delta h_{leaf,m}$ response to T_{act} is similar for all salt concentrations reflecting that the plant behavior is not affected anymore by the solute concentration levels around its roots.

Scenario 2: simulated stress function with a single root

For this scenario, we imposed a constant potential transpiration rate along with a single root located in a soil with different levels of solute concentration. At each time step, an actual transpiration rate and bulk soil averaged potentials or local potentials at the soil-root interface (osmotic, gravimetric and pressure potentials) were obtained.

Comparison with the model of Couvreur et al. 2012

In Fig. 4, the apparent plant stress response ($\alpha = T_{act}/T_{pot}$) is plotted against the total potential (H), the matric potential and gravity potential components ($h + z$), and the osmotic potential (h_o) at the soil-root interface for the lowest transpiration rate, T_{pot}=1.0 cm^3 d^{-1} and for a broad range of initial concentrations. When the soil-root interface total water potential is used, the reduction of the transpiration rate is piecewise linear. It is important to note that neither the initial salt concentration nor the soil type (results not shown) control the shape of these curves. The obtained relation between transpiration rate and total pressure potential at the soil-root interface is identical to the relation proposed by Couvreur et al. (2012), which predicts the onset of stress based on the plant-felt total water potential and predicts a linear decrease of actual T_{act} with the plant felt total water potential. Therefore, a correct evaluation of the root-felt water potential, which is the local total potential at the soil-root interface, is a solution to get a mathematical relationship that depends only on T_{pot} and root properties.

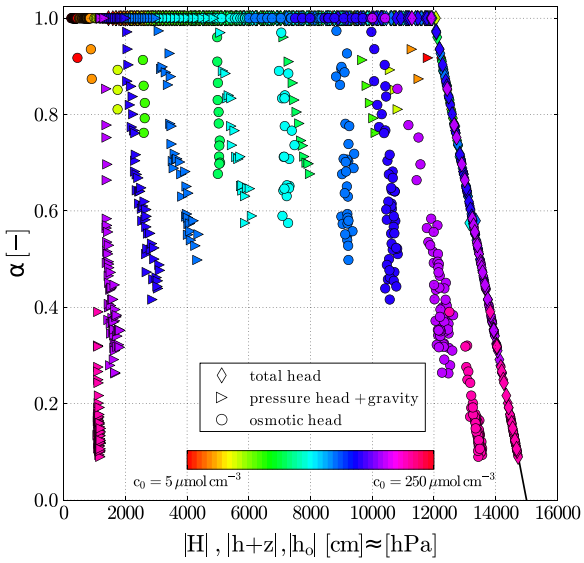

Fig. 4 Transpiration reduction α vs. water potentials at the soil-root interface. Comparison of the total potential $|H|$ (*diamond*) matric plus gravity potential $|h + z|$ (*triangle*) and the osmotic potential $|h_o|$ (*circle*); results are shown for T_{pot}=1 cm^3 d^{-1}. The *colorbar* represents the initial salt concentrations

It can be observed that reduction of the transpiration rate is induced at a very low local negative water potential (−12,000 cm for T_{pot}=1 cm^3 d^{-1}) independently of the main component of the total potential (Fig. 4). Whether the osmotic or the matric component is predominant does not impact the stress onset; only the total water potential is important (given our hypothesis that there is no plant osmotic adjustment and σ=1). This confirms the definition of the model of Couvreur et al. (2012) in which only the total potential is decisive. By comparing the osmotic and matric plus gravity potentials in Fig. 4, it can be seen that both parts can perfectly "compensate" each other.

Comparing Bulk and soil-root interface water potential

In Fig. 5, the reduction functions are plotted either versus the total water potential at the soil-root interface or versus the total water potential of the bulk soil. For a given transpiration rate, the reduction function is clearly not a unique function of the total water potential of the bulk soil but depends strongly on the initial salt concentration or osmotic potential. For lower salt concentrations (Fig. 5a), onset of stress is reached for higher (lower in absolute value) bulk/averaged total water potentials (red-green symbols) than for higher salt concentrations (blue–violet symbols). For higher salt concentrations, the stress response curves obtained using bulk-averaged potentials and using potentials at the soil-root interface approach each other.

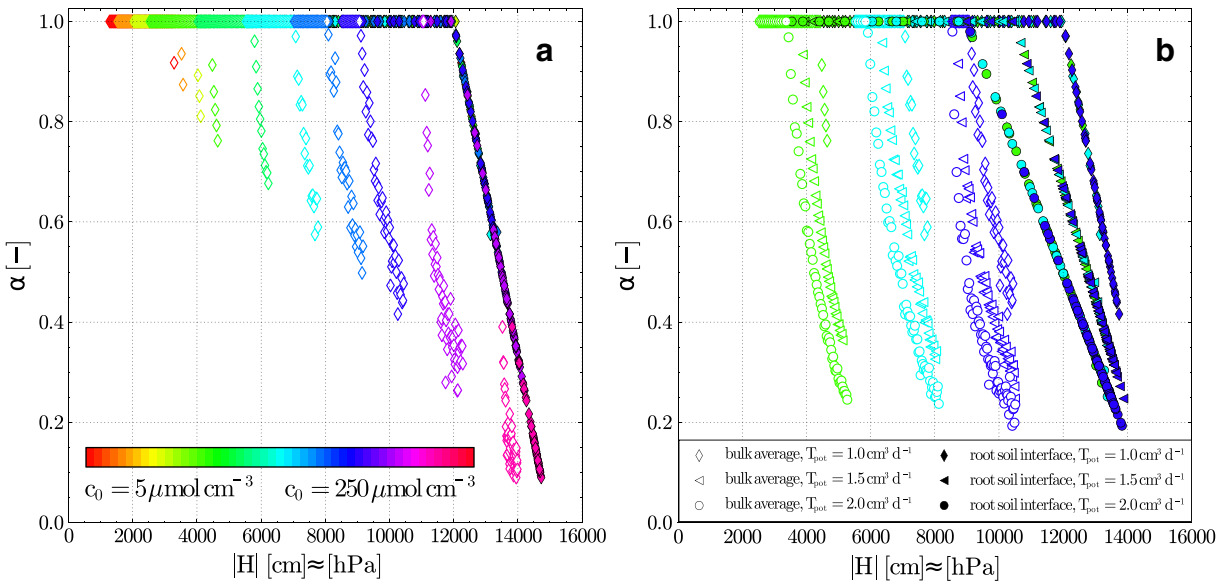

Fig. 5 Reduction function α vs. total water potential $|H|$ at the soil-root interface (*filled symbols*) and vs. total bulk soil water potential (*open symbols*): **a** for T_{pot}=1 cm^3 d^{-1} and the whole considered initial salt concentration range, **b** for three initial salt concentrations and three different transpiration rates (T_{pot}=1.0, 1.5, 2.0 cm^3 d^{-1})

The onset of the reduction and the slope of the reduction function depend on the potential transpiration rate (compare Eq. (4) and Fig. 5b). In addition, the transpiration rate affects the differences between bulk and soil-root interface stress functions (Fig. 5b). A higher transpiration rate leads to a stress onset for less negative bulk soil pressure potentials than the pressure potentials at the root soil interface.

Although local values of the water potential at the soil-root interface should be preferably used for stress functions, they are hardly measurable with current measurement devices. The discrepancy between local and bulk soil water potential is further investigated in Fig. 6, where the total potential at the soil-root interface is plotted against the bulk average total potential. At the beginning of the simulation runs, the solute and water distributions are uniform, leading to no differences between bulk and root surface potentials. With greater simulation time, the gradients of osmotic and matric potential get larger, leading to a larger discrepancy between bulk and soil-root interface potentials. It can be seen that the difference between bulk and soil-root interface water potentials becomes larger with smaller initial solute concentration (see Fig. 5) leading to larger discrepancies between bulk and local stress functions. When stress is reached (here −12,000 cm at the soil-root interface, dashed line in Fig. 6), the difference does not increase further.

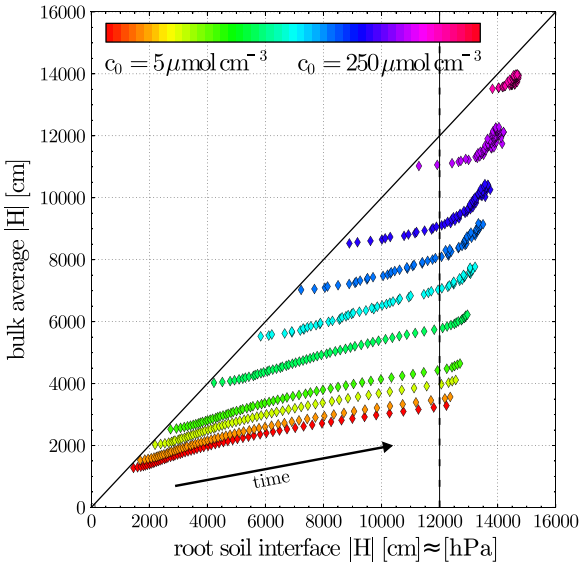

Fig. 6 Average bulk soil total potential |H| vs. total potential at the soil-root interface plotted for different initial concentrations (see *colorbar*) and T_{pot}=1 cm^3 d^{-1}

When comparing the gradients of the matric and osmotic potential that develop in the soil towards the soil-root interface during the simulated time period (Fig. 7), the gradients in matric potential that developed for low initial salt concentration, are much larger than the gradients in osmotic potential that developed for high initial salt concentration. The processes that lead to the development of these two different gradients are fundamentally different. For the matric potential, the gradients drive the water flow in the soil and, because of the non-linearity of the hydraulic conductivity, the gradients have to become very large to drive the same flow when the soil dries out. In porous media where no ion-selective membranes are present, osmotic potential gradients do not drive a liquid water flow but are the result of an advective flow towards the soil-root interface that is countered by a back diffusion. The consequence of this difference in gradients between osmotic and matric potentials is that the difference between soil-root interface total potential and bulk soil total potential depends on which of the components of the water potential (osmotic or matric) is dominating. This implies that, although the relation between the local soil-root interface total potential and transpiration reduction, α, is not dependent on the contribution of osmotic and matric potentials to the total potentials, the relation between the averaged bulk soil total potential and transpiration reduction is because the different potential gradients create different averaged bulk soil potentials.

Indeed, when the soil-root interface water potential depends mainly on solute accumulation around roots and on the matric potential gradient linked to the transpiration rate, the bulk potential is mainly affected by the initial soil water potential and initial salt concentration. By increasing the initial solute concentration, the total bulk soil potential decreased and smaller salt accumulation (and thus a smaller osmotic potential difference between bulk and interface) is needed to generate stress (see Fig. 7). The total bulk water potential is then closer to the soil-root interface total water potential. On the other hand, when the initial salt concentration is low, the matric potential is the major component of the total potential and larger differences exist between root interface and bulk soil matric potential than for the osmotic potential.

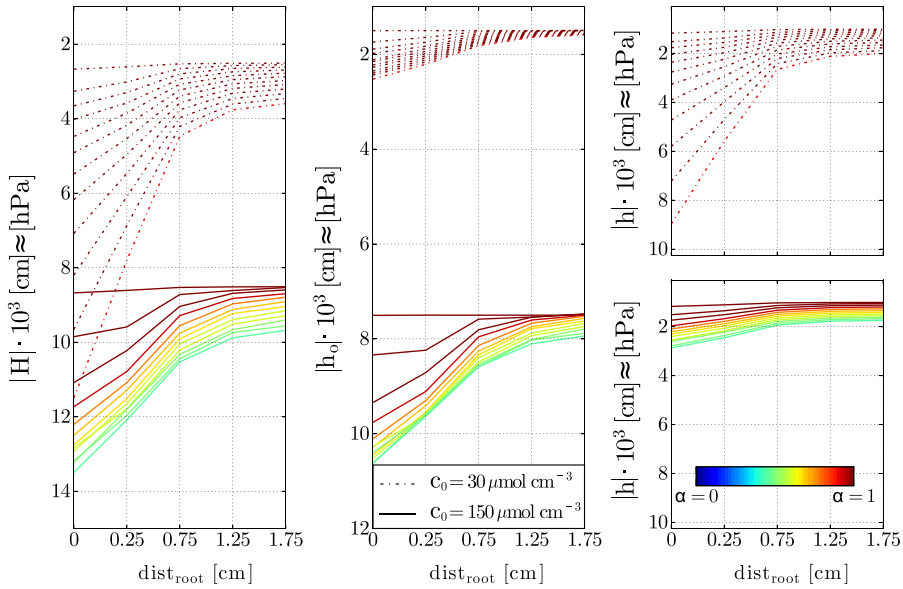

Fig. 7 Distance plots of total potential $|H|$ (*left*), osmotic potential $|h_0|$ (*middle*), and matric potential $|h|$ (*right*) versus distance from the root surface $dist_{root}$ at different times for the single root scenarios; initial concentration c_0=30 μmol cm^{-3} (*dotted line*) and 150 μmol cm^{-3} (*solid line*); T_{pot}=1 cm^3 d^{-1} The *color of each line* represents the transpiration reduction factor which decreases with time

Scenario 3: extrapolation with a full root architecture

Scenario 2 investigated the sensitivity of the stress function to the definition of the water potential (at soil-root interface versus bulk) for a very simple root architecture. It is however to be expected that the difference between stress functions defined in terms of local or bulk potentials will depend on the root distribution, soil type, and transpiration. In this third scenario, we tested the behavior of the stress function with a bigger plant root architecture (Fig. 1b). In this simulation, a sinusoidal day-night cycle of the potential transpiration was used. Therefore, according to Eq. (4) the relation between soil water potential and the reduction coefficient α is not unique anymore since it depends on the potential transpiration rate T_{pot}. This dependency on the potential transpiration is also reported by experimental data (Groenveld et al. 2013). In contrast, the relation Eq. (3), which links the actual transpiration rate T_{act} to the water potential at the soil-root interface, does not depend on T_{pot} (Couvreur et al. 2012) and is used for this scenario (Fig. 8).

Although the local stress function (with the water potential at the soil-root interface) is linear, using the bulk soil potential leads to a non-linear stress response (Fig. 8), as in the single root simulations. The onset of stress also occurs at lower absolute total bulk water potentials than water potentials at the soil-root interface.

However, the difference in the response to bulk averaged or to soil-root interface potentials is not as large in the grassland setup as in the single root scenario. This is

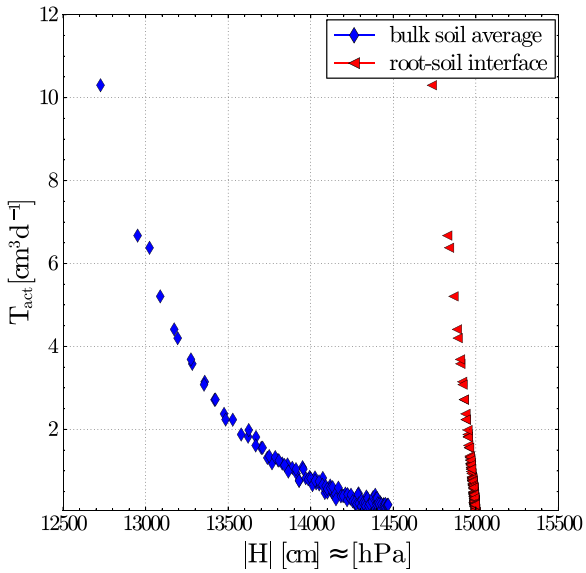

Fig. 8 Actual transpiration T_{act} vs. absolute total potential $|H|$ at the soil-root interface (*triangles-red*) and in the bulk soil (*diamonds-blue*) for the plant root architecture (25 days old)

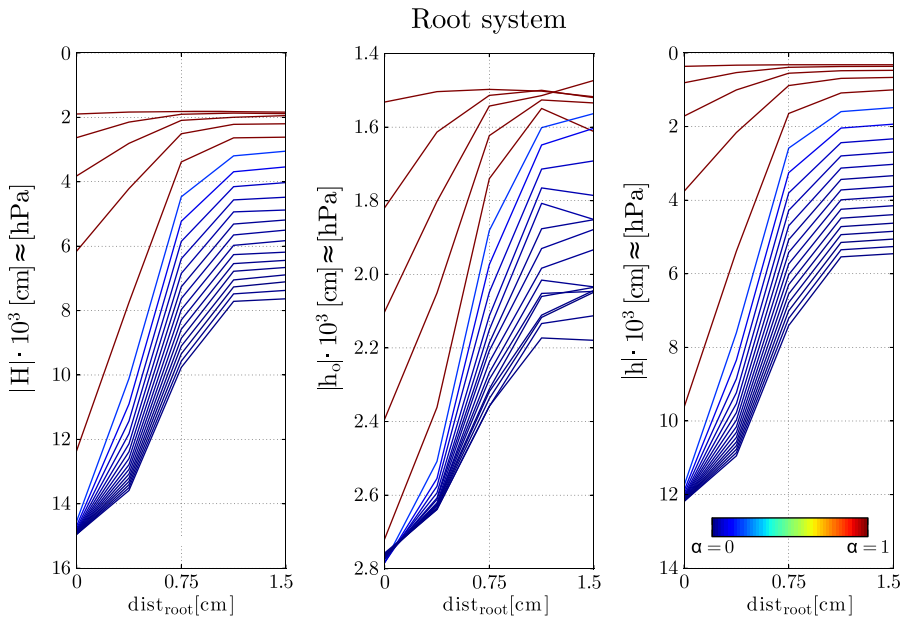

Fig. 9 Total potential $|H|$, osmotic potential $|h_o|$, matric potential $|h|$ versus distance to the nearest root root in the whole plant root structure. The transpiration reduction increases with time (smaller α-see *color bar*)

due to the fact that roots are spread throughout the whole soil column. Although there are still large matric and osmotic potential gradients between root surface and the soil in this scenario (Fig. 9), the average of water potentials includes far more soil voxels close to roots compared to the single root setup. As compared to the single root scenario, this leads to a smaller shift between the bulk averaged and soil-root interface water potentials and shows that the shift between average and soil-root interface water potential depends on the root length density.

Comparison of simulation results with empirical stress functions

Using the averaged total water potential over the root zone and over the complete time period, as is mostly done for experimental data (Dudley and Shani 2003), the transpiration reduction against the bulk soil average water potential is plotted in Fig. 10a for the single root scenario. Here, each point corresponds with one initial concentration and one initial potential transpiration rate.

For each potential transpiration rate, one global transpiration reduction response function can be observed (grey lines). Thus, the global transpiration reduction functions also depend on the potential transpiration rate, as the local transpiration reduction (Fig. 10a—black lines). Note that this was also suggested in the original Feddes water stress function (Feddes et al. 1978).

For the two larger transpiration rates, stress is observed for very small salt concentration in the soil column over the whole simulation period. Hence, the matric potential decrease over the time causes a transpiration reduction and the stress in scenarios with salt is a combination of salt and water stress.

For global transpiration reduction causes by salt only, the single root scenarios were run again, but with additional irrigation uniformly applied at the top soil boundary. The irrigation included salt concentration equal to the initial concentration in the soil and was defined as 2/3 of the T_{pot}. Figure 10b shows the global stress functions for these irrigation scenarios. Here, no stress is observed when the salt concentration is small.

The global transpiration reduction functions are similar to the *s*-shaped salt stress response function of van Genuchten and Hoffman (1984)

$$\alpha = \frac{T_{act}}{T_{pot}} = \frac{1}{1 + \left(\frac{h_o}{h_{o50}}\right)^p} \tag{8}$$

where at h_{o50} is the value of h_o at which the yield, or averaged actual transpiration rate, has declined by 50 % and p is a shape parameter. This shows that the

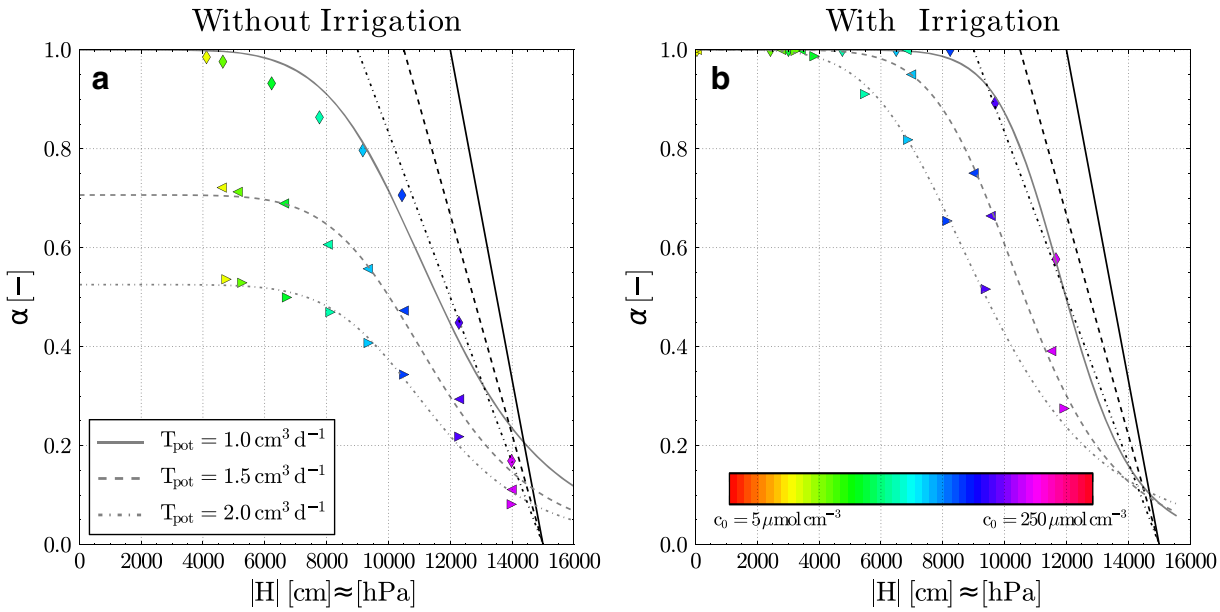

Fig. 10 Time averaged transpiration reduction α plotted versus time and root zone averaged water potential, $|H|$, (*filled symbols-grey lines*), and instantaneous transpiration reduction plotted against the total water potential at the soil-root interface, $|H|$ (piecewise linear functions-*black lines*) for the transpiration rates T_{pot}=1.0 cm^3 d^{-1} (*solid line*), 1.5 cm^3 d^{-1} (*dashed line*) and 2.0 cm^3 d^{-1} (*dotted line*) and the scenarios without irrigation (**a**) and with irrigation (**b**)

piecewise linear local response to stress at every time point is very different from the whole plant response over a longer time period.

Which empirical stress function, which of the stress function parameters, and which combined stress function, fits best must be investigated in further studies. However, as already pointed out by Skaggs et al. (2006), parameters that are obtained by fitting an empirical salt stress function to time-integrated measurement data should not be transferred to numerical models where the response to plant stress is applied at any point and time in the root zone. Using the piecewise linear stress function at the soil-root interface (Eq. (3), black lines in Fig. 10) for every time step, an *s*-shape global stress response is obtained after averaging in time and space.

The relation between local and global transpiration responses depends, among other things, on root length density and soil and root hydraulic parameters, and needs further investigation by analyzing the sensitivity to these parameters.

Summary and conclusion

A coupled numerical model that simulates flow and transport in the soil towards roots and water flow within the root system was used to simulate root water uptake in a drying saline soil with decreasing osmotic and matric potentials. In a first scenario, the simulation results showed a good agreement with the observed data of Hamza and Aylmore (1992). Their study provides experimental information about the relation between solute accumulation at a single root surface, the transpiration rate, and leaf water potential response. The good agreement between the measurements and simulation results indicated that the assumptions of a perfectly selective permeable membrane, negligible osmotic potential of the xylem sap, and no regulation of plant hydraulic properties, were appropriate.

Second, different simulation setups were used to investigate the transpiration response due to water and/or salt stress. The simulation results demonstrated that the actual transpiration rate under stress conditions is linearly related to the local total water potential (sum of matric, gravimetric, and osmotic potentials) at the soil-root interface. This result supports the macroscopic model or type II model of Couvreur et al. (2012), which uses a linear relation between the transpiration rate and a weighted sum of local total water potentials.

However, local water potentials at the soil-root interface were found to differ considerably from bulk water potentials in the root zone. We showed that the differences between soil-root interface and bulk water

potential increased with decreasing root density, decreasing initial salt concentration, and increasing transpiration rate. Furthermore, the differences also depend on the soil hydraulic properties, which also change the gradient between soil-root interface and bulk water potential (Gardner 1960; Schröder et al. 2008), but this was not investigated in this study.

Looking at the relation between the transpiration rate and bulk total water potential, we found that it depends on the composition of the bulk water potential and changes for the same bulk total water potential when the fraction of the bulk osmotic and matric potentials changes. This is a result of different gradients in osmotic and matric potential around a root. As a consequence, the effect of bulk matric and osmotic potentials on water uptake is not additive in contrast to the effect of these potentials at the soil-root interface. Another noticeable difference is that, although stress relations are piecewise linear functions of the local soil-root interface potential, nonlinear relations were obtained when spatially and temporally averaged bulk water potentials were related to temporally averaged transpiration rates.

The fact that the relation between bulk water potential and transpiration rate is influenced by several properties of the soil-plant system (e.g. soil hydraulic properties, root density, root conductivity), and states of the system (e.g. the relation depends on relative contribution of osmotic vs. matric potentials to the total bulk water potential), means that a relation that was parameterized for certain conditions is not directly transferable to other conditions. This may also explain the large noise that is often observed in experimentally derived relations (Homaee et al. 2002a, b, c). When soil hydraulic properties are known and root distributions, salt and water contents are measured, simulations using a more detailed process model, which considers small scale variations of matric potentials and osmotic potentials (or salt accumulation) around roots, may be used to derive root hydraulic properties by inverse modeling. In a subsequent step, simulation by such a detailed model may be used to derive stress relations in terms of bulk soil water potentials in response to other conditions. In future work, the relation between local and global transpiration reduction must be analyzed, and their dependence an plant and soil parameters, e.g., root length density and soil and root hydraulic parameters, should also be investigated. In addition, the simulations in this study focused on salt accumulation around plant roots and did not consider salt uptake. Nevertheless, some salts are taken up by plants and the amount and mechanisms of the salt uptake influence the concentration distribution around the root system (Schröder et al. 2012). Furthermore, we assumed no osmotic adjustment, but implementing such an adjustment in the model is straightforward. Root hydraulic properties, osmotic potential of the xylem sap, and the reflection coefficient of the osmotic membrane σ can be made functions of external and internal conditions (e.g. water potentials). It is more difficult to set up experiments and measure responses that can be used to validate and parameterize such functions. However, model simulations may be an useful first step to assess the sensitivity of the system to such adjustments. In a second step, simulations can be used to design experiments that can be used to parameterize adjustment functions.

Acknowledgments This work was partly funded by the I-CORE Program of the Planning and Budgeting Committee and the Israel Science Foundation (Grant 152/11).

Appendix: model description

The model R-SWMS simulates both, soil and root water flow. Soil water flow is defined by the Richards equation (Richards 1931)

$$\frac{\partial \theta}{\partial t} = \nabla[\mathbf{K}(h)\nabla(h+z)] - S(x,y,z) \tag{9}$$

where θ [L^3 L^{-3}] is the volumetric water content, t [T] is time, $\mathbf{K}$ [L T^{-1}] is the hydraulic conductivity tensor, h [L] is the matric potential, S [T^{-1}] is a sink term representing the root water uptake, and z [L] is the vertical coordinate positive upward. The model of (Doussan et al. 1998) is coupled to the soil water flow. This model calculates water flow inside the roots based on a root network architecture, which is described as a network of connected root nodes. The axial xylem flow J_x [L^3 T^{-1}] in a root segment describes water flow within the root xylem by

$$J_x = -K_x^* A_x \left(\frac{\Delta h_{xylem}}{l_{seg}} + \frac{\Delta z}{l_{seg}} \right) \tag{10}$$

where K_x^* [L T^{-1}] is the xylem conductivity, A_x [L^2] is the xylem cross-sectional area, z [L] the vertical coordinate, l_{seg} [L] the root segment length, and h_{xylem} [L] the water pressure potential in the xylem.

The radial water flow J_r [L^3 T^{-1}] between the soil-root interface and the root xylem is defined by Doussan et al. (1998) and used in R-SWMS as

$$J_r = K_r^* A_r \left(H_{int} - H_{xylem}\right) \tag{11}$$

with the radial root conductance K_r^* [T^{-1}], the root outer surface A_r [L^2] and the water potential at the soil–root interface H_{int} [L] and in the xylem H_{xylem} [L].

The calculations of soil and root water flow inside R-SWMS are coupled as described in Javaux et al. (2008) via the water sink term S in the Richards equation and defined for one soil voxel by

$$S_j = \frac{\sum_{k=1}^{n_k} J_{r,k}}{V_j} \tag{12}$$

where J_k is the radial fluxes into the root segment k, located in a soil voxel j. Here, V_j is the voxel volume, and n_k is the number of root segments within voxel j.

The solute movement inside the soil is described by the convection–dispersion equation (CDE)

$$\frac{\partial \theta c}{\partial t} = \nabla(\theta D \cdot \nabla c) - \nabla(\theta u c) - S' c \tag{13}$$

where c [M L^{-3}] is the solute concentration, u [L T^{-1}] is the pore water velocity, S' [T^{-1}] is the solute sink term and D [L^2 T^{-1}] is the dispersion coefficient tensor, defined as

$$D_{ij} = \lambda_T \|u\| \delta_{ij} + (\lambda_T - \lambda_L)\frac{u_j u_i}{\|u\|} + D_w \tau \delta_{ij} \tag{14}$$

where $\|u\| = \sqrt{uu^T}$ is the Euclidean norm of the pore water velocity vector, α_L and α_T are the longitudinal and transverse dispersivities, respectively, D_W [L^2 T^{-1}] is the molecular diffusion coefficient and τ [−] is the tortuosity factor.

The CDE is solved by the model PARTRACE (Bechtold et al. 2011; Schröder et al. 2012). PARTRACE solves a random walk particle tracking algorithm, where an equivalent stochastic differential definition of the CDE is used, which contains the velocity provided by R-SWMS and a random displacement which accounts for the dispersion. A large number of solute particles represent the solute mass and are moved through the system according to this equation.

With an interface between R-SWMS and PARTRACE, velocity and water sink term profiles are updated in every time step and provided to the solute transport code. In addition, after the concentration profile is calculated by PARTRACE, a feedback coupling supply the concentration values, which are transformed to osmotic potentials, to the soil and root water module of the model (R-SWMS).

References

Bechtold M, Vanderborght J, Ippisch O, Vereecken H (2011) Efficient random walk particle tracking algorithm for advective-dispersive transport in media with discontinuous dispersion coefficients and water contents. Water Resour Res 47, W10526

Bhantana P. and Lazarovitch N. (2010) Evapotranspiration, crop coefficient and growth of two young pomegranate (Punica granatum L.) varieties under salt stress. Agric. Water Manage. doi:10.1016/j.agwat.2009.12.016

Cardon G, Letey J (1992) Plant water uptake terms evaluated for soil water and solute movement models. Soil Sci Soc Am J 32:1876–1880

Couvreur V, Vanderborght J, Javaux M (2012) A simple three-dimensional macroscopic root water uptake model based on the hydraulic architecture approach. Hydrol Earth Syst Sci 16:2957–2971

de Jong van Lier QD, van Dam JC, Metselaar K, de Jong R, Duijnisveld WHM (2008) Macroscopic root water uptake distribution using a matric flux potential approach. Vadose Zone J 7:1065–1078. doi:10.2136/vzj2007.0083

De Wit C (1958) Transpiration and crop yields. Versl Landbouwk Onderz 64. 6. Universtity Wageningen.

Doussan C, Pagès L, Vercambre G (1998) Modelling of the hydraulic architecture of root systems: an integrated approach to water absorption—model description. Ann Bot 81:213–223

Doussan C, Pierret A, Garrigues E, Pagès L (2006) Water uptake by plant roots: II—modelling of water transfer in the soil root-system with explicit account of flow within the root system—comparison with experiments. Plant Soil 283:99–117

Dirksen C, Kool JB, Koorevaar P, van Genuchten MT (1993) HYSWASOR- simulation model of hysteretic water and solute transport in the root zone. In: Water flow and solute transport in soils. Springer Berlin, Heidelberg, pp 99–122. doi:10.1007/978-3-642-77947-3_8

Dudley LM, Shani U (2003) Modeling plant response to drought and salt stress reformulation of the root-sink term. Vadose Zone J 2:751–758

Feddes R, Raats P (2004) Parameterizing the soil-water-plant root system. In: Feddes R, de Rooij G, van Dam J (eds) Unsaturated-zone modeling: progress, challenges and applications. UR Frontis Series, Wageningen, pp 95–141

Feddes R, Kowalik P, Kolinska-Malinka K, Zaradny H (1976) Simulation of field water uptake by plants using a soil water dependent root extraction function. J Hydrol 31:13–26

Feddes R, Kowalik P, Zaradny H (1978) Simulation of field water use and crop yield. 188

Gardner W (1960) Dynamic aspects of water availability to plants. Soil Sci 89(2):63–73

Groenveld T, Ben-Gal A, Yermiyahu U, Lazarovitch N (2013) Weather determined relative sensitivity of plants to salinity: quantification and simulation. Vadose Zone J. doi:10.2136/vzj2012.0180

Hainsworth J, Aylmore L (1986) Water extraction by single plant roots. Soil Sci Soc Am J 50:841–848

Hamza M, Aylmore L (1992) Soil solute concentration and water uptake by single lupin and radish plant roots. Plant Soil 145: 187–196

Homaee M, Dirksen C, Feddes RA (2002a) Simulation of root water uptake: I. Non-uniform transient salinity using different macroscopic reduction functions. Agric Water Manag 57:89–109

Homaee M, Feddes RA, Dirksen C (2002b) A macroscopic water extraction model for nonuniform transient salinity and water stress. Soil Sci Soc Am J 66:1764–1772

Homaee M, Feddes R, Dirksen C (2002c) Simulation of root water uptake: III. Non-uniform transient combined salinity and water stress. Agric Water Manag 57:127–144

Hopmans J, Bristow K (2002) Current capabilities and future needs of root water and nutrient uptake modeling. Adv Agron 77:104–175

Jarvis NJ (2011) Simple physics-based models of compensatory plant water uptake: concepts and eco-hydrological consequences. Hydrol Earth Syst Sci 15:3431–3446

Javaux M, Schröder T, Vanderborght J, Vereecken H (2008) Use of a three-dimensional detailed modeling approach for predicting root water uptake. Vadose Zone J 7(3): 1079–1088

Knipfer T, Fricke W (2010) Root pressure and a solute reflection coefficient close to unity exclude a purely apoplastic pathway of radial water transport in barley (Hordeum vulgare). New Phytol 187:159–170

Kroes J, van Dam J, Groenendijk P, Hendriks R, Jacobs C (2008) SWAP version 3.2. In: Theory description and user manual. Wageningen, The Netherlands, p 262

Maas E, Hoffman G (1977) Crop salt tolerance-current assessment. J Irrig Drain Div 103:115–134

Metselaar K, de Jong van Lier Q (2007) The shape of the transpiration reduction function under plant water stress. Vadose Zone J 6:124–139. doi:10.2136/vzj2006.0086

Nassar IN, Horton R (1997) Heat, water, and solute transfer in unsaturated porous media: I—theory development and transport coefficient evaluation. Transp Porous Media 27: 17–38

Nimah MN, Hanks RJ (1973) Model for estimating soil water, plant, and atmospheric interrelations: I. Description and sensitivity. Soil Science Society of America Journal pp 522–527

Pagès L, Vercambre G, Drouet J (2004) Root Typ: a generic model to depict and analyse the root system architecture. Plant Soil 258:103–119

Richards LA (1931) Capillary conduction of liquids through porous mediums. Physics 1(5):318

Schröder T, Javaux M, Vanderborght J, Körfgen B, Vereecken H (2008) Effect of focal soil hydraulic conductivity drop using a three-dimensional root\water uptake model. Vadose Zone J 7:1089–1098

Schröder N, Javaux M, Vanderborght J, Steffen B, Vereecken H (2012) Effect of root water and solute uptake on apparent soil dispersivity: a simulation study. Vadose Zone J 11(3). doi: 10.2136/vzj2012.0009

Shani U, Ben-Gal A (2005) Long-term response of grapevines to salinity: osmotic effects and ion toxicity. Am J Enol Vitic 52: 148–154

Siebert S, Burke J, Faures JM, Frenken K, Hoogeveen J, Döll P, Portmann FT (2010) Groundwater use for irrigation—a global inventory. Hydrol Earth Syst Sci 14(10):1863–1880

Simunek J, Sejna M, Saito H, Sakai M, van Genuchten MT (2013) The HYDRUS-1D software package for simulating the movement of water, heat, and multiple solutes in variably saturated media. HYDRUS Softw 3, Department of Environmental Sciences, University of California Riverside, Riverside, California, USA

Skaggs TH, van Genuchten MT, Shouse PJ, Poss JA (2006) Macroscopic approaches to root water uptake as a function of water and salinity stress. Agric Water Manag 86:140–149

Tardieu F (1996) Drought perception by plants. Do cells of droughted plants experience water stress? Plant Growth Regul 20:93–104. doi:10.1007/BF00024005

van Genuchten M (1980) A closed-form equation for predicting the hydraulic conductivity of unsaturated soils. Soil Sci Soc Am J 8:892–898

van Genuchten M (1987) A numerical model for water and solute movement in and below the root zone. United States Department of Agriculture Agricultural Research Service U.S. Salinity Laboratory

van Genuchten M, Hoffman G (1984) Analysis of crop salt tolerance data. In: Soil Salinity under Irrigation. Processen and Management. Springer Verlag, New York, pp 251–271

Van Genuchten M, Leij F, Yates S (1991) The RETC code for quantifying the hydraulic functions of unsaturated soils. Riverside, California: EPA Report 600/2-91/065, U.S. Salinity Laboratory, USDA, ARS.